

# Localization at irrational fillings in the Aubry-André model

Balázs Hetényi<sup>1,2</sup> and István Balogh<sup>1</sup>

<sup>1</sup>*MTA-BME Quantum Dynamics and Correlations Research Group,  
Department of Physics,  
Budapest University of Technology and Economics,  
H-1111 Budapest, Hungary*

<sup>2</sup>*Institute for Solid State Physics and Optics,  
Wigner Research Centre for Physics,  
H-1525 Budapest, P. O. Box 49, Hungary*  
(Dated: September 4, 2024)

We calculate the phase diagram of the Aubry-André model as a function of filling and potential strength ( $W$ ). We apply periodic boundary conditions and calculate the geometric Binder cumulant to determine the transition between the extended and localized phases. For rational fillings the phase transition occurs at  $W = 2t$  ( $t$  denotes the hopping parameter), but spikes occur in the phase diagram at fillings which correspond to ratios of Fibonacci numbers. In the thermodynamic limit these ratios tend to specific irrational numbers, and  $W \rightarrow 0$  at these fillings. We also calculate the phase diagram of an extended Aubry-André model with second nearest neighbor hoppings. In addition to spikes, this phase diagram also exhibits discontinuities (jumps) at some of the irrational fillings at which the spikes occur.

*Introduction.-* The delocalization-localization transition (DLT) occurring in disordered [1–3] and quasiperiodic [4–6] systems is a topic of ongoing interest. Recent experimental developments allow the manipulation of ultracold atoms in optical lattices and enable the direct examination of the predicted localization phenomena. Billy et al. experimentally studied [7] Anderson localization in a Bose-Einstein condensate (BEC), while Roati et al. directly observed [8, 9] the duality of the Aubry-André model [4] (AAM) in a BEC in a quasiperiodic optical lattice. The AAM is equivalent to the Harper model [10], which is the canonical model in the study of the quantum Hall effect [11–13]. The AAM, exhibits a DLT at finite potential strength. Jitomirskaya showed [14] that for  $W > 2t$  (Eq. 1) all states become exponentially localized. Recent studies [15, 16] argue for refining this result. Based on an investigation of the inverse participation ratio, Wang et al. [15] argue that for  $W < 2t$  states near the band edge are “almost localized”. Zhang et al. [16], based on considering wave number dependence, reach the same conclusion. Extended [17–21] AAMs exhibit, in addition to localized and extended phases, a critical phase. Recently, twisted bilayer graphene (Moiré system) was studied [20] via an extended AAM derived by dimensional reduction. This study used a renormalization group (RG) approach [22] to calculate the phase diagram.

In this work we calculate the phase diagram of the AAM as a function of particle density (filling) and  $W/t$ . We study the model under periodic boundary conditions (PBC). In topological insulators, topological invariants [13, 23, 24] are defined under PBC. Generalized AA models [25] give rise to Majorana fermions [26], which are of topological origin. Small periodic chains [27] (rings), of interest on their own, exhibit a wealth of in-

teresting phenomena [21, 28, 29], such as multifractality [21, 28]. An AAM ring study by Dey et al. [29] suggests that such systems can be used as high-to-low conductivity switches by varying the filling. Similar behavior was demonstrated [30] in an AAM model assembled from electric circuit elements. Our studies confirm this, but we also show that the conduction properties depend crucially on whether the filling corresponds to a rational or an irrational number. To gauge localization and to determine the DLT we use the geometric [31–33] Binder cumulant [34, 35] (GBC), a tool rooted in the modern polarization theory [36–39] (MPT).

Our calculations concur with the original predictions [4, 14] (a transition at  $W/t = 2$ ) for rational particle density (filling), but for irrational fillings we find that the AAM is localized. This manifests in “spikes”, isolated points where the transition occurs at  $W/t < 2$  (Fig. 1). At these spikes the filling is a ratio of Fibonacci numbers (or a sum of such ratios). As the system size is increased, these ratios tend to specific irrational numbers. Our extrapolation study of the critical  $W$  shows that  $W \rightarrow 0$  (via power law decay), meaning that at these irrational fillings the system is localized at any  $W > 0$ . This conclusion is corroborated by a position space renormalization group study, developed [40] specifically for applications within an MPT context. We also calculate the LDT for an extended AAM, which exhibits discontinuities in its DLT phase diagram.

*Model and calculation details.-* We consider a Hamiltonian of the Aubry-André type given by

$$\hat{H} = -t \sum_{j=1}^L (c_{j+1}^\dagger c_j + c_j^\dagger c_{j+1}) + W \sum_{j=1}^L \xi_j n_j, \quad (1)$$

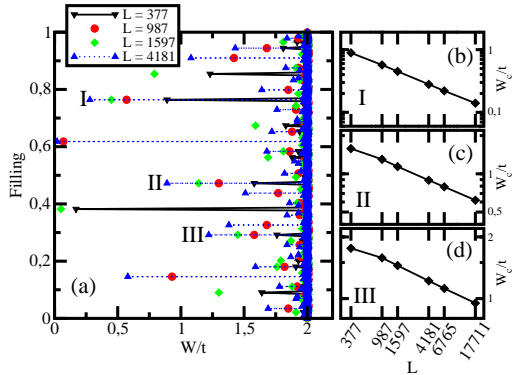


FIG. 1. Panel (a) on the left shows the calculated phase diagram for four different system sizes,  $L = 377, 987, 1597, 4181$ . The predicted  $W/t = 2$  line is found for most fillings, but all system sizes exhibit spikes where the localization transition occurs at  $W/t < 2$ . The right panels ((b), (c), and (d)) show the critical  $W$  for three spikes of system size for six different sizes,  $L = 377, 987, 1597, 4181, 6765, 17711$ . The spikes are labeled in panel (a) as I, II, and III. In the plots for the three spikes, (b), (c), and (d), the scales of all axes are logarithmic.

where  $\xi_j = \cos(2\pi\alpha j)$ , where  $\alpha$  is the golden ratio obtained from the ratio of consecutive members of the Fibonacci sequence in the limiting case, and the operators  $c_j^\dagger(c_j)$  create(annihilate) a particle at site  $j$ . For finite systems with PBC, the irrational  $\alpha$  is approximated as a ratio  $\alpha \approx F_{n+1}/F_n$ , where  $F_n$  is the  $n$ th Fibonacci number, so the size of the system can not be smaller than  $F_n$ , otherwise the potential would not be "smooth". In our calculations  $L = F_n$ .

We diagonalize  $\hat{H}$  under PBC, meaning that we obtain a set of states on the lattice,  $\Phi_\lambda(j)$ , where  $\lambda$  denotes the state index, and  $j$  denotes the lattice site. For a system with  $N$  particles, the ground state wave function is a Slater determinant consisting of the  $N$  states,  $\Phi_\lambda(j)$ ,  $\lambda = 1, \dots, N$  with lowest energy,

$$\Psi(j_1, \dots, j_N) = \text{Det} [\Phi_\lambda(j_\mu)], \quad (2)$$

where  $j_\mu$  denotes the lattice coordinate of particle  $\mu$ , and  $\mu = 1, \dots, N$ . To construct the GBC, one first calculates the quantity  $Z_q$ , defined in the case of band systems as

$$Z_q = \text{Det} \left[ U_{\lambda\lambda'}^{(q)} \right], \quad (3)$$

where

$$U_{\lambda\lambda'}^{(q)} = \sum_{j=1}^L \phi_\lambda^*(j) \exp\left(i\frac{2\pi q}{L}j\right) \phi_{\lambda'}(j). \quad (4)$$

Using  $Z_q$  we can define the approximate second and

fourth order statistical cumulants as

$$C_2 = M_2 = \frac{L^2}{2\pi^2}(1 - |Z_1|) \quad (5)$$

$$C_4 = \frac{L^4}{8\pi^4}(-|Z_2| + 4|Z_1| - 3),$$

From which we can define the GBC as

$$U_4 = -\frac{1}{3} \frac{C_4}{C_2^2}, \quad (6)$$

which is a known gauge of the localization transition in this and other models.  $U_4$  is equivalent to the *excess kurtosis*, a ratio of cumulants used in statistics to characterize the tails of probability distributions. Its advantage here is that it changes sign at DLT. We exploit this feature in our calculations below. We also define the distribution of the total position  $X$  as the Fourier transform of  $Z_q$ ,

$$P(X) = \frac{1}{\sqrt{L}} \sum_{q=0}^{L-1} Z_q \exp\left(i\frac{2\pi q}{L}X\right) \quad (7)$$

*Energy levels.*- Fig. 2 shows the energy levels as a function of  $W/t$  for a system of size  $L = 610$ . Only states with energies below zero are shown, since the upper half is symmetric to the lower half. The  $W/t$ -axis is logarithmic, which makes the other symmetry, which originates from the duality of the model, explicit (symmetry around  $W = 2t$ ). As  $W$  is increased from zero, gaps are seen to open. In Fig. 2 the uppermost states for three filled bands are indicated. The state indices are at  $I_{state} = 89, 123, 233$ , two of which are Fibonacci numbers, the remaining one is the sum of two Fibonacci numbers. Not all gaps are visible in the figure, other gaps can be seen by zooming in.

*Even vs. odd  $N$  and  $L$ .*- Before presenting our results of the phase diagram, we need to address the issue of odd versus even system size and particle number. We find that when  $N$  and  $L$  are either both even or odd, the distribution of the periodic total position  $X$  (defined in Eq. (7)) is bimodal near the critical  $W/t$ . Fig. 3 shows results for system size  $L = 987$ , an odd system size. Panels (a) and (b) show results for  $N = 737$  while panels (c) and (d) show results for  $N = 738$ . Panels (a) and (c) are for  $W/t = 1.98$  in the delocalized phase, while panels (b) and (d) are for  $W/t = 2.02$ , in the localized phase. Most importantly, in the localized phase, we see that the odd particle number system ( $N = 737$ ) shows two clearly separated peaks, whereas the system with  $N = 738$  shows only one peak within one  $L = 987$  system. In other example calculations we performed we always find that if the system size and particle number are either both even or both odd, the distribution in the localized phase is bimodal. In this case the GBC formalism ( $U_4$ ) is not applicable. However, in cases in

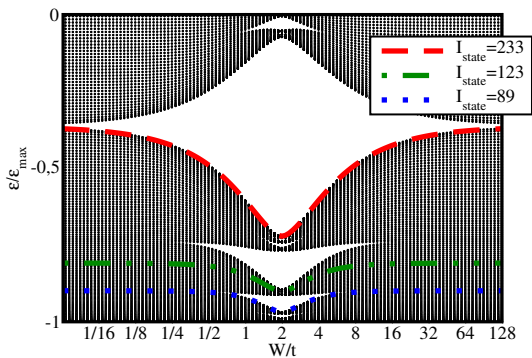


FIG. 2. Energy levels of the Aubry-André model for a system of size  $L = 610$  with periodic boundary conditions as a function of  $W/t$ . Only states with  $\epsilon < 0$  are shown, since the system is symmetric with respect inversion around  $\epsilon = 0$ . The scale of the  $W/t$  axis is logarithmic. Band gaps are found at states whose indices correspond to Fibonacci numbers or sums of Fibonacci numbers.

which the even versus odd parity of system size and particle number are different, we always find single peaks, and the GBC formalism is applicable. Even though the GBC formalism (as derived in this work) is not applicable to the even/even and odd/odd cases, it is still possible to determine the DLT critical point by direct observation of  $P(X)$ . This is somewhat laborious, so below we focus on systems in which the even vs. odd parities between  $L$  and  $N$  are different, where  $U_4$  is a reliable indicator of the DLT. We have also carried out calculations in which the parities are the same and found that the conclusions stated below, regarding irrational spikes in the phase diagram, are maintained.

*Phase diagram and spikes.*- The phase diagram obtained from our GBC calculations is shown in Fig. 1, in the main panel of that figure, for four system sizes,  $L = 377, 987, 1597, 4181$ , all odd Fibonacci numbers. The scan in particle number includes all even  $N$ . The phase diagram shows many examples of the predicted  $W/t = 2$ , but spikes are also seen, where  $W/t < 2$ . At these spikes  $W/t$  decreases with increasing system sizes. Fillings at such spikes tend to specific irrational numbers which can be calculated by taking the limit of the particular Fibonacci ratios.

In Fig. 1a we labelled three spikes I, II, and III. For I, the filling can be written as  $N/L = 2F_{n-2}/F_n$ . As the system size is increased (as  $n \rightarrow \infty$ )  $N/L \rightarrow 3 - \sqrt{5}$ . Fig. 1b the critical value of the interaction strength is shown as a function of system size, for  $L = 377, 987, 1597, 4181, 6765, 17711$ , covering almost two orders of magnitude. In Figs. 1b, 1c, 1d, all axes are logarithmic. The three plots are all well approximated by straight lines, suggesting that the critical potential strength decreases to zero in the thermodynamic limit according to a power law. We fitted

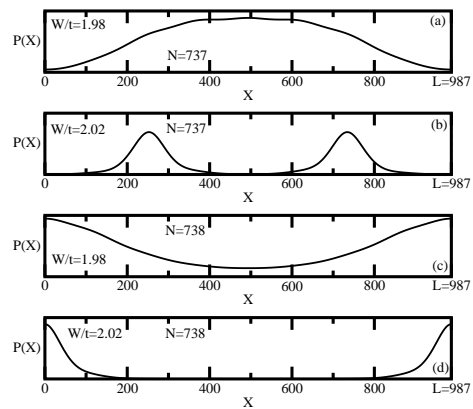


FIG. 3.  $P(X)$ , distribution of the total position  $X$ , for four different calculations of system size  $L = 987$ . Panels (a) and (b) show the results for  $N = 737$ . Panel (a)(panel (b)) shows results for  $W/t = 1.98(W/t = 2.02)$ . Panels (c) and (d) show results for  $N = 738$ . Panel (c)(panel (d)) shows results for  $W/t = 1.98(W/t = 2.02)$ .

the function  $f(L) = aL^{-b}$  to the data shown in Fig. 1a and found  $a = 15.3(4)$  and  $b = 0.479(4)$ . The spikes indicated by labels II and III (results shown in Figs 1c and Fig. 1d) exhibit the same features. For spike II  $N/L = \lim_{n \rightarrow \infty} \frac{F_{n-2} + F_{n-5}}{F_n} \rightarrow 2\sqrt{5} - 4$ ,  $a = 7.6(1)$ ,  $b = 0.257(2)$ , for spike III  $N/L = \lim_{n \rightarrow \infty} (2F_{n-5}/F_n) \rightarrow 7 - 3\sqrt{5}$  and  $a = 5.36(5)$  and  $b = 0.177(1)$ . Other spikes we checked also occur at irrational fillings which can be derived from the formula for the Fibonacci sequence, and they approach a critical  $W/t = 0$  asymptotically.

The emerging picture is that the phase diagram depends crucially on whether the filling is rational or irrational,  $W/t = 2$  for the former, and  $W/t = 0$  for the latter. All fillings turn into spikes as the system size is increased. This is due to the fact that all numbers can be written as the sum of Fibonacci numbers (even unity is a Fibonacci number). Suppose that one starts with a system size  $L = F_n$ , then the filling  $F_1/F_n$  will exhibit a transition at  $W/t = 2$ . If we increase the system size, and study the "same" filling, in other words we calculate  $U_4$  for the sequence  $F_2/F_{n+1}, F_3/F_{n+2}, \dots$  (we increase the index of both Fibonacci numbers by the same integer) the transitional  $W$  will eventually go to zero, according to a power law. At the same time, since the system size has increased, there will be new fillings for which the transition takes place at  $W/t = 2$ . Those fillings correspond to rational numbers which are not yet good approximations to the irrational number to which they correspond in the limit of large  $L$ .

*Polarization renormalization.*- It is possible to apply RG methods [22, 41] to quasi-periodic systems. One such approach [22] is based on increasing the unit cell of commensurate approximants. In a recent work an MPT based renormalization group approach was devel-

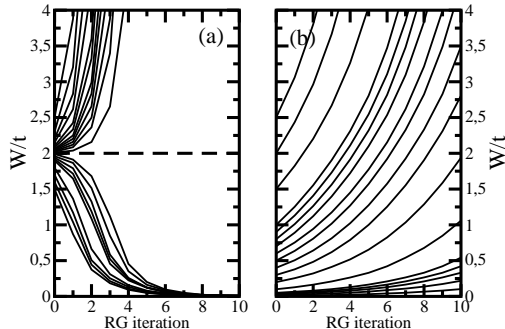


FIG. 4. Flow lines generated by renormalization of the polarization amplitude. Panel (a) shows a calculation for half filling. The iterations were carried out between  $L = 2584$  and  $L = 610$ . The dashed line ( $W = 2t$ ) indicates a repulsive fixed point. The flowlines originating below(above)  $W = 2t$  tend to the attractive fixed point at  $W = 0$  ( $W \rightarrow \infty$ ). Panel (b) shows a calculation for an irrational filling ( $\lim_{n \rightarrow \infty} 2F_{n-2}/F_n$ ). The iterations were carried out between the two systems  $L = 1597$ ,  $N = 1220$  and  $L = 987$ ,  $N = 754$ . In this case  $W = 0$  ( $W \rightarrow \infty$ ) is a(n) repulsive(attractive) fixed point. Flow lines started at finite  $W$  all tend to infinity, indicating localization.

oped [40], which we adopt here in such a way that rational and irrational fillings can be distinguished. The idea is to apply decimation to the expectation value of the twist operator,  $Z_1$ . The approach generates a flow in the parameters of the Hamiltonian. The flow equations can exhibit fixed points (repulsive or attractive). In our case, one can generate a flow in  $W$  by iterating the following equation,

$$|Z_1(W_{j+1}, N', L')| = |Z_1(W_j, N, L)|, \quad (8)$$

where the approach of Ref. [40] was modified by including the particle number  $N$  as a variable. In practice, this equation translates to the following: one starts with a value of the potential strength,  $W_0$ , and calculates  $Z_1$  for a system with particle number  $N$ , and system size  $L$ . One then finds the  $W_1$  that gives the same value of  $Z_1$  for a smaller system with particle number  $N'$  and size  $L'$ . In the next step, one uses  $W_1$  again, to calculate  $Z_1$  for the  $N, L$ -system. In this case the iteration generates a flow in  $W$ . The key feature is that it is possible to distinguish rational and irrational fillings. For a rational filling, one keeps the particle number so that  $N/L$  is fixed during the iteration. For irrational filling one has to make the ratios  $N/L$  and  $N'/L'$  correspond to different approximations of the desired irrational filling, the  $N'/L'$  being the one closer to the desired number.

In Fig. 4 two examples are shown, one for a filling of  $1/2$  (rational filling), the other for a filling of  $2F_{n-2}/F_n \rightarrow 3 - \sqrt{5}$ . For the former, we used the two system sizes,  $L = 2584$  and  $L = 610$ , since we needed the

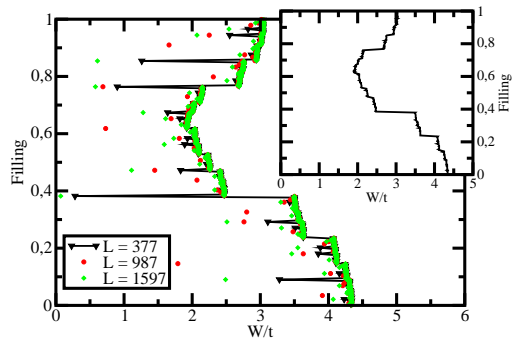


FIG. 5. Phase diagram of the extended Aubry-André model, with second nearest neighbor hopping with strength  $t_2 = 0.5$ . Calculations based on three system sizes ( $L = 377, 987, 1597$ ) are shown. Fillings with even particle number were scanned. The main panel shows a full calculation, with spikes included. The spikes correspond to fillings which tend to irrational numbers in the thermodynamic limit. The predicted phase diagram for rational fillings is shown in the inset.

system sizes to be even. For the latter, we used  $L = 1597$  and  $L = 987$ . Fig. 4a shows a flow diagram exhibiting two attractive fixed points ( $W = 0$  and  $W \rightarrow \infty$ ) and one repulsive fixed point at  $W = 2t$ . The flow diagram for irrational filling (Fig. 4b) exhibits an attractive fixed point at  $W \rightarrow \infty$  and a repulsive one at  $W = 0$ . It is of interest to note that, while the GBC finds critical values of  $W$  at finite values (which extrapolate to  $W = 0$  for large system sizes), the RG approach generates flow lines which immediately show that the localization transition occurs at  $W = 0$ .

*Extended Aubry-André model.*- Extensions of the Aubry-André model constitute a very broad topic[17–19, 21, 27, 28, 42, 43]. Here we treat a simple extension, namely the model defined in Eq. (1) with an additional term consisting of second nearest neighbor hopping,

$$\hat{H}_2 = -t_2 \sum_{j=1}^L (c_{j+2}^\dagger c_j + c_j^\dagger c_{j+2}), \quad (9)$$

again, with PBC. The phase diagram is shown in Fig. 5 for three odd system sizes ( $L = 377, 987, 1597$ ). The phase diagrams were generated by scanning through even  $N$ s. Spikes for found at irrational fillings, but in addition to Fig. 1, there are also discontinuous "jumps" (horizontal in the figure) which also occur at irrational fillings. Almost all such discontinuities we observe are accompanied by spikes. The inset shows the phase diagram based only on rational fillings. It is worthwhile to compare our results in the inset to two previous studies, Refs. [43] and [42]. Both phase diagrams are shown in Fig. 4 of Ref. [42], albeit, ours is upside down compared to those results, because we took the sign of the hoppings to be negative. The results shown in Fig. 4

of Ref. [42] are approximate, in particular the results of Ref. [42] show considerable error bars. Comparing our results, however, to those of Ref. [43] (also shown in Fig. 4 of Ref. [42]), we see that both exhibit discontinuities in the same places, although, ours are more pronounced. Those of Ref. [43] appear to be smeared out.

*Conclusion.-* We studied the Aubry-André model under periodic boundary conditions using techniques which can simultaneously treat rational and irrational fillings, but distinguish their behavior. We find that for rational fillings the well-known results,  $W = 2t$ , are recovered, but for irrational fillings there is no delocalized phase. Our work has interesting implications for generalizations of the AA model as well as for quantum Hall studies, for which known studies, based on the TKNN [13] invariant, only handle the case of rational flux. The implications of our results for quantum Hall systems would be interesting. The state of affairs we find also suggests the use of this model in

the construction of high-to-low conductivity switches, an effect predicted [29] in small Aubry-André rings. Our methods are definitely applicable to related disordered models in which the distinction between rational and irrational filling may be of interest, for example generalizations of the AA model, models with uncorrelated or correlated disorder, or other quasiperiodic models, such as the Fibonacci chain [44].

## ACKNOWLEDGMENTS

BH was supported by the National Research, Development and Innovation Fund of Hungary within the Quantum Technology National Excellence Program (Project Nr. 2017-1.2.1-NKP-2017-00001) grant nos. K142179 K142652 and by the BME-Nanotechnology FIKP grant (BME FIKP-NAT).

- 
- [1] E. Abrahams, P. W. Anderson, D. C. Licciardello, and T. V. Ramakrishnan, *Phys. Rev. Lett.* **42** 673 (1979).
- [2] A. Langedijk, B. van Tiggelen, and D. S. Wiersma, *Physics Today* **62** 24 (2009).
- [3] F. Evers and A. D. Mirlin, *Rev. Mod. Phys.* **80** 1355 (2008).
- [4] S. Aubry and G. André, *Ann. Isr. Phys.* **3** 133 (1980).
- [5] A. J. Martinez, M. A. Porter, and P. T. Kevrekidis, *Philos. Trans. A* **376** 20170139 (2018).
- [6] G. A. Dominguez-Castro, R. Paredes, *Eur. J. Phys.* **40** 045403 (2019).
- [7] J. Billy, V. Josse, Z. Zuo, A. Bernard, B. Hambrecht, P. Logan, D. Clément, L. Sanchez-Palencia, P. Bouyer, and A. Aspect, *Nature (London)* **453** 891 (2008).
- [8] G. Roati, C. D'Errico, L. Fallani, M. Fattori, C. Fort, M. Zaccanti, G. Modugno, M. Modugno, and M. Inguscio, *Nature (London)* **453** 895 (2008).
- [9] M. Modugno, *New. J. Phys.* **11** 033023 (2009).
- [10] P. G. Harper, *Proc. Phys. Soc. A* **68** 874 (1955).
- [11] K. von Klitzing, G. Dorda, and M. Pepper, *Phys. Rev. Lett.* **45** 494 (1980).
- [12] D. C. Tsui, H. L. Stormer, and A. C. Gossard, *Phys. Rev. Lett.* **48** 1559 (1982).
- [13] D. J. Thouless, M. Kohmoto, M. P. Nightingale, M. den Nijs, *Phys. Rev. Lett.* **49** 405 (1982).
- [14] S. Ya. Jitomirskaya, *Ann. Math.* **150** 1159 (1999).
- [15] Y. Wang, G. Xianlong, and S. Chen, *Eur. Phys. J. B* **90** 215 (2017).
- [16] Y. Zhang, D. Bulmash, A. V. Maharaj, C.-M. Jian, and S. A. Kivelson, arXiv:1504.05205.
- [17] S. Ganeshan, J. H. Pixley, and S. Das Sarma, *Phys. Rev. Lett.* **114** 146601 (2015).
- [18] J. Biddle and S. Das Sarma, *Phys. Rev. Lett.* **104** 070601 (2010).
- [19] A. Padhan, M. K. Giri, S. Mondal, and T. Mishra, *Phys. Rev. B* **105** L220201 (2022).
- [20] M. Gonçalves, B. Amorim, E. V. Castro, and P. Ribeiro, *Phys. Rev. Lett.* **131** 186303 (2023).
- [21] M. Dziurawiec, J. O. de Almeida, M. L. Bera, M. Plodzień, M. M. Maška, M. Lewenstein, T. Grass, and U. Bhattacharya, *Phys. Rev. B* **110** 014209 (2024).
- [22] M. Gonçalves, B. Amorim, E. V. Castro, and P. Ribeiro, *Phys. Rev. B* **108** L100201 (2023).
- [23] B. A. Bernevig and T. L. Hughes, *Topological Insulators and Superconductors*, Princeton University Press (2013).
- [24] J. K. Asbóth, L. Oroszlány, and A. Pályi, *A Short Course on Topological Insulators: Band Structure and Edge States in One and Two Dimensions*, Lecture Notes on Physica, vol. 919, Springer International Publishing, (2016).
- [25] S. Ganeshan, K. Sun, and S. Das Sarma, *Phys. Rev. Lett.* **110** 180403 (2013).
- [26] A. Yu. Kitaev, *Phys.-Usp.* **44** 131 (2001).
- [27] E. Papp and C. Micu, *Low-Dimensional Nanoscale Systems on Discrete Spaces*, World Scientific, Singapore, (2007).
- [28] C. Monthus, *Fractals* **27** 1950007 (2017).
- [29] S. Dey, D. Daw, S. K. Maiti, *EPL* **129** 47002 (2020).
- [30] S. Ganguly and S. K. Maiti *Sci. Rep.* **13** 13633 (2023).
- [31] B. Hetényi and B. Dóra, *Phys. Rev. B* **99** 085126 (2019).
- [32] B. Hetényi and S. Cengiz, *Phys. Rev. B* **106** 195151 (2022).
- [33] B. Hetényi, submitted.
- [34] K. Binder, *Z. Phys. B* **43** 119 (1981).
- [35] K. Binder, *Phys. Rev. Lett.* **47** 693 (1981).
- [36] R. D. King-Smith and D. Vanderbilt, *Phys. Rev. B* **47** R1651 (1993).
- [37] R. Resta, *Rev. Mod. Phys.* **66** 899 (1994).
- [38] D. Vanderbilt, *Berry Phases in Electronic Structure Theory*, Cambridge University Press, Cambridge, U.K. (2018).
- [39] R. Resta, *J. Phys.: Cond. Mat.* **12** R107 (2000).

- [40] B. Hetényi, S. Parlak, and M. Yahyavi, *Phys. Rev. B* **104** 214207 (2021).
- [41] M. Wilkinson, *Proc. Roy. Soc. Lond. A* **391** 305 (1984).
- [42] V. Kerala Varma and S. Pilati, *Phys. Rev. B* **92** 134207 (2015).
- [43] J. Biddle, D. J. Priour Jr., B. Wang, and S. Das Sarma, *Phys. Rev. B* **83** 075105 (2011).
- [44] A. Jagannathan, *Rev. Mod. Phys.* **93** 045001 (2021).